AIAA JOURNAL
Vol. 45, No. 6, June 2007

# Spatial Correlations in a Transonic Jet

Lawrence Ukeiley*
*University of Florida, Shalimar, Florida 32579*
Charles E. Tinney†
*Université de Poitiers, 86034 Poitiers, France*
Richa Mann‡
*University of Mississippi, University, Mississippi 38677*
and
Mark Glauser§
*Syracuse University, Syracuse, New York 13244*

DOI: 10.2514/1.26071

**Particle image velocimetry measurements of an unheated Mach 0.85 jet are used to examine its various turbulence properties. The data are presented from two separate experiments; one with the light sheet orientated in the streamwise direction ($r$–$x$ plane) and one with the light sheet perpendicular to the flow direction ($r$–$\theta$ plane). The instrument's characteristics allow for the calculation and subsequent analysis of the two-point spatial correlations which are known to be relevant to the source terms in acoustics analogies where sound production is concerned. An examination of the spatial correlations demonstrates the averaged spatial evolution of the jet's large-scale turbulent structures throughout the noise producing region. In particular, the ($r$–$x$) spatial dependence of the axial and azimuthal normal stresses manifest a oblique structure in the mixing layer regions of the flow, whereas the radial normal stresses evolve more uniformly toward the end of the potential core. Quadrupole source terms relevant to the sound production mechanisms are also calculated from which their spatial distributions are analyzed with zero time delay. The analysis of these source terms at $x/D = 4$ show how the peak energy for the shear-noise component resides on the high-speed side of the shear layer around $r/D = 0.33$, whereas the self-noise terms peak along the lip-line at $r/D = 0.5$, and are most energetic for the streamwise and azimuthal components of the velocity. To fully evaluate the quadrupole sources of noise, the space-time correlations of the full three-dimensional turbulent flowfield are required which are currently not available from experiments.**

## I. Introduction

THE noise generated by the turbulent fluctuations of high-speed, transonic jet plumes represents an important source of sound for many civilian and military aircraft personnel, especially those who reside and work in close proximity to active aviation operations. Fundamental studies of these sources have been ongoing essentially since the advent of jet aircraft and have concentrated on both the turbulent flow and the acoustic pressure fluctuations that it radiates. Although several decades of research have produced numerous volumes of literature pertaining to the subject of aerodynamically generated noise, many scientific gaps still reside in identifying the exact nature by which turbulent flows generate sound. Particularly challenging is the limited information identifying the differences between the turbulent statistics of the "quiet" and "noisy" structures of a flow [1,2], and under what circumstances do some of the dynamic characteristics (of the flow) play a more significant role than others. In hindsight, the recent advancements with computational capabilities, including the introduction of planar optical techniques, have provided the necessary tools by which identifying (and controlling) the sources of sound from high-speed jet flows may be addressed.

Lighthill [3,4] has been attributed with developing the first theory by which the turbulent properties of a flow could generate and emit sound. Since this work, there has been a wealth of studies using numerical, analytical, and experimental techniques, most of which have improved the capabilities of existing tools for capturing and understanding the so-called sources of noise. Many reviews of Lighthill's original work have been performed, including those of Crighton [5], Ffowcs-Williams [6], Goldstein [7], Ribner [8], and Lilley [9], to name a few. In Lighthill's analogy [3,4], the turbulence field is replaced by a volume of distributed sources with equivalent energy. As is known, the Lighthill analogy allows one to solve for the far-field sound using sources which comprise properties of an unsteady fluid in free space. It is believed that this accounts for all of the effects of the fluid flow, including the interaction of the sound field with the turbulence. However, the exact mechanisms by which the rotational hydrodynamic energy of the turbulence is transferred into irrotational propagative energy is still unknown. This is primarily due to the fact that a complete evaluation of the radiating sources of noise in turbulent flows requires not only a three-dimensional survey of the turbulent structures, but also their temporal behavior. This of course has been very challenging for the experimentalist, thus placing most of the demand for understanding the noise source mechanisms into the hands of the numerical community.

With the advancement of the personal computer, the ability to accurately model turbulent flows has increased substantially. Thus, time-dependent numerical simulations have been used to examine the so-called noise sources in subsonic and supersonic turbulent shear flows for many reasons, including their ability to model all regions of space and time. These include both direct numerical simulations [2,10] and large eddy simulations [11]. Colonius and

Presented as Paper 2654 at the 34th AIAA Fluid Dynamics Conference and Exhibit, Portland, Oregon, 28 June–1 July 2004; received 21 June 2006; revision received 26 December 2006; accepted for publication 26 January 2007. 

*Assistant Professor, Mechanical and Aerospace Engineering. AIAA Senior Member.
†Postdoctoral Research Fellow, Centre National de la Recherche Scientifique, Laboratoire d'Etudes Aerodynamiques, Poitiers, France. AIAA Member.
‡Graduate Student, Aeroacoustics Emphasis on Engineering Science, Jamie L. Whitten National Center for Physical Acoustics.
§Professor, Mechanical and Aerospace Engineering, 151 Link Hall. Associate Fellow AIAA.

Freund [12], Freund [2], and Whitmire and Sakar [13] have demonstrated the ability to validate the Lighthill approach using numerical simulations. In particular, Freund [2] concentrated on both confirming one's ability to calculate the far-field noise from the turbulence and an identification of the properties associated with this noise. However, the exact process by which noise is generated still remains to be fully understood and has prompted many new concerns regarding the robustness of the acoustic analogy [14] (such as the Lighthill [3], Goldstein [15], and Lilley [16] analogies) and the assumptions of the turbulent correlations and statistics [9,17]. Thus, the capabilities for evaluating these assumptions, as well as verifying the acoustic analogy directly, has been underway [14,18].

Returning once more to the experimental community, developing an understanding of the turbulent fluctuations in shear flows and the means by which they generate and radiate sound into the acoustic far field has been an understudy almost since the original work of Lighthill [3,4]. Some of these studies comprise multipoint measurements of various fluid properties (velocity, pressure) and surveys of the far-field acoustics. However, since the advent of laser-based optical techniques, the ability to measure the turbulent properties of unsteady fluid motions without intruding on the natural characteristics of the flow has substantially improved the capabilities of the experimentalist and his/her contribution to the aeroacoustics field. This, along with the limited use of hot wires (Harper-Bourne [19]) has shifted the measurements from mean properties, as was historically done with pressure-based probes, to terms more relevant to those which arise in the theories of aerodynamically generated sound. Lau et al. [20] and Morris [21] used laser Doppler velocimetry (LDV) techniques to measure turbulence properties in compressible jets and are attributed to extending these measurement techniques to transonic regimes. Complementary to the aforementioned investigations, Stromberg et al. [22] and Ukeiley et al. [23,24] employed rakes of hot wires to show the similarities and differences in the compressible flow structure to their incompressible counterparts. Where planar-based optical techniques are concerned, such as particle image velocimetry (PIV), Seiner et al. [25], Arakeri et al. [1], and Bridges and Wernet [26,27] have illustrated the spatial properties of the turbulence structure throughout the dominant sound producing regions of the jet. Additional precursors to these later studies have added a wealth of understanding regarding the spatial correlations of the turbulent jet, which forms the basis of Lighthill's acoustic analogy [3,4].

Although the aforementioned studies have concentrated on either measuring the near-field velocity or far-field sound independently, some attempts have been undertaken to relate the two through synchronous measurements. These pioneering efforts date back to the 1970s, whereby hot-wire (velocity) and microphone (far-field noise) measurements were acquired simultaneously. Based on the causality principles of Siddon [28], only limited success was achieved, notably due to the low levels of correlations between the two fields (velocity and acoustic midfield). However, others [29–31] have had success in separating the "shear-noise" component of the turbulence from "self-noise," where the peak of the jet's primary sources of noise are concerned, the former component being dominant. Recently, these types of studies have been reinstated using more advanced planar optical techniques to measure the flowfield [32]. In addition to these studies, PIV measurements have been acquired synchronously with the far-field acoustics [33] which will be studied in a later part of this larger effort.

In this study, we concern ourselves with an examination of the turbulent velocity field from a high Reynolds number, Mach 0.85 jet, acquired using stereo particle image velocimetry techniques. This tool is used to measure the velocity field in two planes: 1) aligned with the primary jet flow direction ($x$–$r$), and 2) perpendicular to the primary jet flow ($r$–$\theta$). The measurements concentrate on mapping out a region up to ten jet exit diameters $D$ downstream of the nozzle exit plane, comprising the near-field region of the jet, the collapse of the potential core, and the region after the potential core where the dominant sound producing events are commonly believed to originate. In the analysis, terms relevant to the Lighthill source tensor [3,4] are examined and contrasted with previous assumptions which were necessary where limited sampling capabilities and data storage were more concerning. Because PIV yields snapshots of highly resolved spatial data uncorrelated in time (preemptive to time-resolved PIV instruments which are still incapable of sampling at adequate speeds to resolve all of the scales of the flow at these speeds), we will only be able to examine the spatial correlations, not the space-time correlations. The latter of the two is crucial in determining the acoustic far-field noise from the turbulence. However, this is an initial part of a larger study where experimentally estimated time-dependent data [33] will be available and these methods will be alluded to.

## II. Experimental Facilities and Techniques

The experimental results reported in this work were collected in facilities both at the University of Mississippi and Syracuse University (see Fig. 1a). The two facilities each have unique features in terms of capabilities and instrumentation. In what follows, some of the highlighted capabilities will be detailed.

### A. Anechoic Jet Laboratory

The Anechoic Jet Laboratory is housed in the Jamie Whitten National Center for Physical Acoustics (NCPA) on the campus of the

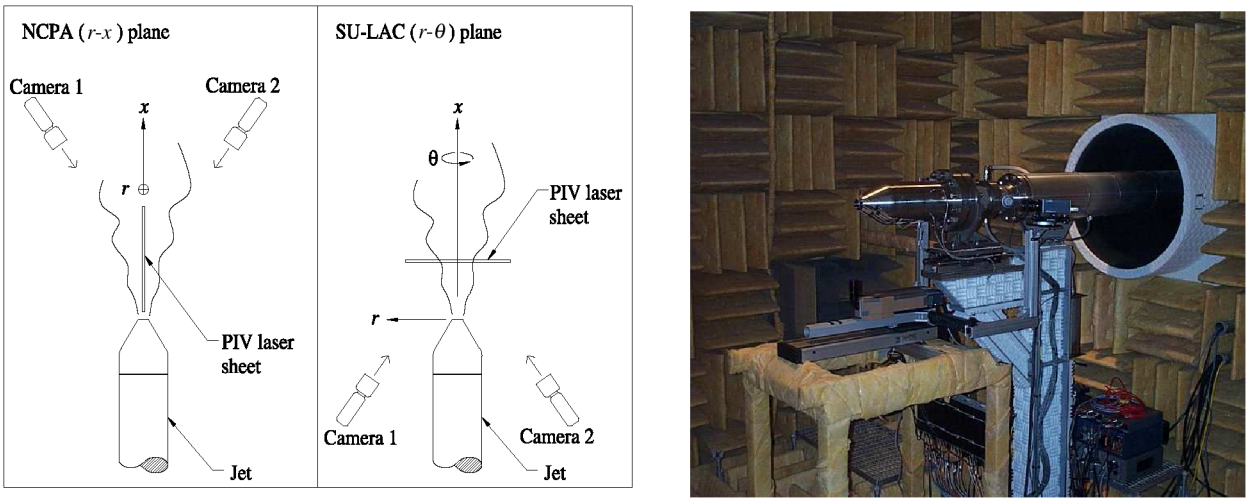


a) b)

**Fig. 1 a) PIV arrangements at University of Mississippi and Syracuse University, and b) anechoic chamber with nozzle and instrument configuration at Syracuse University.**

University of Mississippi. Details of this facility can be found in Ponton et al. [34]. The fully anechoic chamber encompasses 14.3 $m^3$ (within the fiberglass wedge tips), comprising a sound absorption coefficient of at least 0.99 for all frequencies above 200 Hz. A powered ventilation system provides uniform airflow (~0.3 m/s) via plenums located behind the front and rear walls. The compressed air system is capable of providing over 6000 SCFM (standard cubic feet per minute) of dry (−40°C dewpoint) air at 600 psia in conjunction with over 170 $m^3$ of air storage space to damp out any fluctuations from the compressor system. A combination of different valves allows the exit Mach number to be held constant within 1% and a muffler system removes any excess noise introduced by the valves. Additional characteristics include a liquid propane burner (although not employed in this study), a ceramic flow straightener (400 cells/$in^2$), and a converging nozzle with an exit diameter of 3.56 cm.

The measurements presented here for discussion were acquired using a three-component PIV system, comprising Kodak ES 1.0 cameras [8 bit, 9 mm charge-coupled device (CCD) array of 1008 × 1016 pixels] used to capture suspended atomized mineral oil illuminated by a New Wave-Gemini laser. Timing of the system is handled by the IDT Flex controller and the images are either processed using a commercial software package from IDT or with an in-house code (EDPIV). Details of the algorithms for data processing in each of these can be found in Gui and Wereley [35] and Wereley and Gui [36]. The atomized mineral oil is introduced upstream of the plenum using a Laskin nozzle-based system, capable of producing particles on the order of 1 $\mu$m in diameter.

The flow conditions consisted of a cold, Mach 0.85 jet (based on centerline exit velocity $U_{cl}$) corresponding to a Reynolds number of $7.4 \times 10^5$. The initial shear layer thickness based on pitot-tube measurements at the jet exit was estimated to be $0.0180D$. The measurements presented from this facility, orientated the PIV light sheet parallel to the jet axis, from which 1000 image pairs were acquired (at each of the four streamwise positions) to study the streamwise $x$ and radial $r$ properties of the flow simultaneously. Further details of the experiments and an uncertainty analysis of the data has been reported in Mann [37]. The overall uncertainty in the streamwise component of the velocity was estimated to peak at values nearly 4 m/s for these experiments. The zero in the coordinate system for both facilities was chosen to be at the center of the jet's exit plane. At each of the four locations, the camera's spatial window captured approximately two to three jet exit diameters, as is shown in Fig. 2a using the axial mean profile as an example. Although overlapping measurement windows between all of the zones could provide further confirmation of the current results, this was only accomplished for zones 3 and 4 between 9 and 10 diameters downstream of the jet exit (see Fig. 2). In this region, it was determined that the mean streamwise velocity between the two measurement windows agreed to within 5% typically. The distance between the cameras and the laser light sheet was dictated by the relationship between pixel size and particle size. The velocity components $\tilde{u}_i$ are denoted by streamwise $\tilde{u}_1$, radial $\tilde{u}_2$, and azimuthal $\tilde{u}_3$, whereby mean and fluctuating components are simply obtained from the decomposition of the instantaneous field: $\tilde{u}_i = U_i + u_i$.

The streamwise and radial mean velocities are shown in Fig. 2 demonstrating the natural growth of the jet's shear layer. Of particular interest is the significant difference between the low-speed side of the shear layer and the entrainment regions of the flow in the mean radial profiles (Fig. 2b). This shows the abundance of air that is entrained by the jet, especially near the nozzle region of the flow.

### B. Large Anechoic Chamber

The large anechoic chamber (LAC) located at Syracuse University (see Fig. 1b) was originally built in the 1970s and has recently undergone substantial rehabilitation, the details of which are discussed in Tinney et al. [38]. The interior of the chamber encloses 206 $m^3$ and is fully anechoic with a cutoff frequency of 150 Hz. Five tanks store 335 $m^3$ of dry (−40°C) compressed air supplied by a two

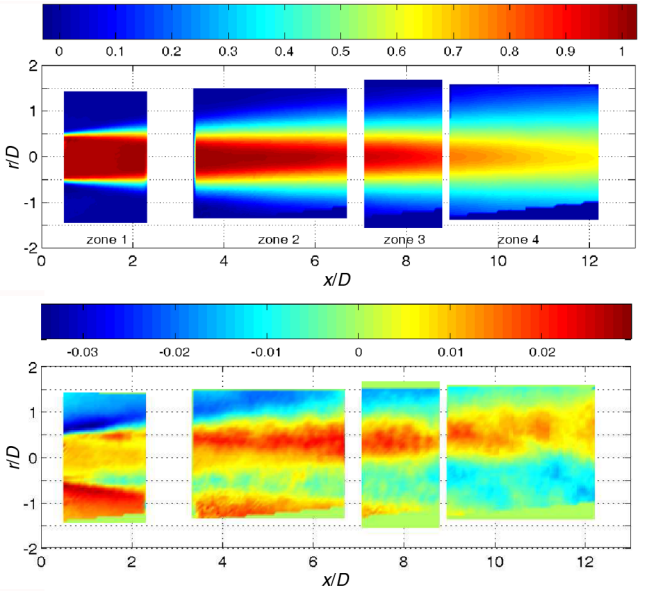


**Fig. 2 Mean profiles of the a) axial ($U_1/U_{cl}$), and b) radial ($U_2/U_{cl}$) components of velocity.**

stage (2 piston) 500 psia compressor. The valve that controls the air speed at the nozzle's exit comprises a whisper trim interior followed by a filter for removing sources of contaminating noise induced by the compressor and control valve. The air system at Syracuse University is equipped with a 470 kW electric circulation heater capable of elevating the exit temperature at the exit of the nozzle for heated jet studies. Behind the chamber, a large plenum feeds temperature controlled air supplied by an industrial make-up-air unit, into the anechoic chamber. After which, both the jet and bypass air are discharged by a centrifugal fan at the aft wall of the anechoic chamber along the same axis of the jet. The nozzle is 5.08 cm in diameter and measurements were acquired at an exit Mach number of 0.85, corresponding to a Reynolds number of $1 \times 10^6$. The initial shear layer thickness based on pitot-tube measurements at the jet exit and $U = 0.95U_{cl}$ was extrapolated and found to be $0.0175D$ [39].

The measurements reported here were acquired using a Dantec Dynamics' three-component PIV system oriented perpendicular to the jet flow $(r, \theta)$ to capture all three components of the velocity field along 21 slices between 3.0 and 8.0 jet diameters ($\delta x/D$= 0.25 increments). Specific information concerning the algorithms for processing and calibration can be found through the Dantec Dynamics web site[¶] as they pertain to the FlowManager software (v3.3). Furthermore, a detailed description of the PIV arrangement, as well as the processing of the PIV data (grid transformation of the PIV vector maps, the jet's turbulent statistics, preservation of the momentum integral, spatial filtering effects) the reader should refer to Sec. II of Tinney et al. [39]. At each of the streamwise locations, 1250 statistically independent image pairs were acquired and used for processing.

## III. Statistics of Noise Sources

It is well known that Lighthill [3,4] developed an expression to describe aerodynamically generated sound by subtracting the divergence of the momentum equation from the time derivative of the continuity equation, which is written as follows:

$$\frac{\partial^2 \rho}{\partial t^2} - a_\infty^2 \frac{\partial^2 \rho}{\partial x_i \partial x_i} = \frac{\partial^2 T_{ij}}{\partial x_i \partial x_j} \tag{1}$$

where the Lighthill stress tensor (or source term) is given by

[¶]http://www.dantecdynamics.com

$$T_{ij} = \rho\tilde{u}_i\tilde{u}_j + \left(p - \rho a_\infty^2\right)\delta_{ij} - \tau_{ij} \tag{2}$$

Here, $a_\infty$ is the ambient speed of sound and $\tau_{ij}$ is the viscous stress tensor. The left-hand side of this inhomogeneous wave, Eq. (1), represents the propagation of the sound after it leaves the turbulent flowfield, whereas the right-hand side is said to be representative of the generation of sound in the turbulent flow. Classically, the last two terms on the right-hand side of the Lighthill stress tensor, Eq. (2), are neglected using a cold jet and high Reynold's number assumptions, respectively, for each of the terms. Freund [10] recently evaluated these assumptions and showed that even in a lower Reynold's number jet, the contribution from the viscous stress tensor is indeed negligible. This, however, was not necessarily the case for the middle term. Because only the velocity field was acquired in the current experiments, we will work with the commonly used assumption that $T_{ij} = \rho\tilde{u}_i\tilde{u}_j$.

The calculation of aerodynamically generated sound is conventionally carried out in one of two ways. The first involves directly evaluating the source field on the right-hand side of Lighthill's equations and using it as a time-dependent input in the solution of Eq. (1). This was carried out by Colonius & Freund [12] and required a large computational effort not only to solve for the nonhomogeneous wave equation, but to process a highly resolved grid that was necessary for adequately modeling the acoustic source terms. This is not possible using the current data set because it has been sampled discontinuously. However, Tinney et al. [40] have presented a method for reconstructing a time-resolved estimate of the flowfield through a mean-square estimation procedure. This tool has demonstrated many promising results and will be the subject of future studies.

The second involves solving Eq. (1) for an analytical solution to the density field. This has been shown previously for an unbounded flow and has the following form:

$$\rho(\boldsymbol{y}, t) \approx \frac{1}{4\pi a_\infty^2} \iiint_V \frac{1}{|\boldsymbol{y} - \boldsymbol{x}|} \frac{\partial^2 T_{ij}(\boldsymbol{x}, \tau)}{\partial x_i \partial x_j}\, \mathrm{d}\boldsymbol{x} \tag{3}$$

where $\rho$ is the density fluctuations in the far field and $\tau$ is now a retarded time coefficient that is associated with the propagation of the sound. This can be rewritten as follows:

$$\rho(\boldsymbol{y}, t) \approx \frac{1}{4\pi a_\infty^4} \frac{x_i x_j}{x^3} \iiint_V \frac{\partial^2 T_{ij}(\boldsymbol{x}, \tau)}{\partial \tau^2}\, \mathrm{d}\boldsymbol{x} \tag{4}$$

where $x_i/x$ is the direction cosine between the source at $\boldsymbol{x}$, and the observation point at $\boldsymbol{y}$. It should be pointed out that in much of the literature on this subject, the direction cosines and $T_{ij}$ are combined so that the equation is written with the second time derivative of $T_{xx}$ using the velocity in the direction of the observation point. However, in instances where PIV data are employed, it may be more convenient to leave it in the form shown in Eq. (4) because the measurements are typically acquired along a discretized Cartesian grid.

Typically, one is concerned with the far-field acoustic intensity,

$$I(\boldsymbol{y}) = \frac{a_\infty^3}{\rho_o} \langle \rho(\boldsymbol{y}, t)^2 \rangle \tag{5}$$

which, after substituting the density field $\rho(\boldsymbol{x}, t)$ in (5) using (4), we can rewrite this as follows:

$$I(\boldsymbol{y}) = \frac{x_i x_j x_k x_l}{16\pi^2 a_\infty^5 \rho_o x^4} \int_V \int_{V'} \left\langle \frac{\partial^2 T_{ij}}{\partial \tau^2} \frac{\partial^2 T'_{kl}}{\partial \tau^2} \right\rangle \mathrm{d}\boldsymbol{x}\, \mathrm{d}\boldsymbol{x}' \tag{6}$$

Here, the first and second terms in the bracket are evaluated at $(\boldsymbol{x}, \tau)$ and $(\boldsymbol{x}', \tau')$ which are suitable retarded times to reach the observation point. Following the analysis of Proudman [41] and later, Ribner [42], the preceding relationship can be written as

$$I(\boldsymbol{y}) = \frac{x_i x_j x_k x_l}{16\pi^2 a_\infty^5 \rho_o x^4} \int_V \frac{\partial^4}{\partial \tau^4} \langle T_{ij} T'_{kl} \rangle\, \mathrm{d}\boldsymbol{r} \tag{7}$$

using several assumptions such as homogeneity of the turbulence field. If one assumes that the only important term in the Lighthill stress tensor is the first, that is $T_{ij} = \tilde{u}_i\tilde{u}_j$, then Eq. (7) can be simplified as

$$I(\boldsymbol{y}) = \frac{x_i x_j x_k x_l}{16\pi^2 a_\infty^5 \rho_o x^4} \int_V \frac{\partial^4}{\partial \tau^4} \langle \tilde{u}_i \tilde{u}_j \tilde{u}'_k \tilde{u}'_l \rangle\, \mathrm{d}\boldsymbol{r} \tag{8}$$

As one can see, the principle term in Eq. (8) comprises fourth-order, two-point, time and space correlations. Of course, other forms to the solution of the Lighthill equation can be derived if different limiting assumptions are applied, many of which result in the two-point correlation as the principle term. An example of this was shown by Seiner et al. [43] who used the properties from algebraic correlations to derive an expression for the far-field intensity. This was obtained by multiplying the double divergence of a Green's function with $T_{ij}T_{kl}$, of which the former needed to be defined. In concert with Eq. (8), these formulations demonstrate the importance for studying the two-point correlations as a means by which to understand and predict the noise sources in unbounded turbulent flows. In Secs. V and VI we will present the two-point spatial correlations from the data sets described in Sec. II.

## IV. Single-Point Turbulent Statistics and the Lighthill Source Term

If one is to solve the Lighthill equation, then one must be able to measure the source term $T_{ij}$. The ability to measure all of the nine terms in this tensor, from which the double divergence is calculated, has been central to many of the complicating factors in studying the noise sources generated by turbulence. Throughout the results sections we will present turbulence properties as they relate to the Lighthill source tensor.

First, we will examine some of the individual components of the simplified form of $T_{ij}$, i.e., $u_i u_j$ using a subset of the data acquired at the NCPA. The density term has been dropped here, and will be neglected throughout the Results section due to the lack of available local density measurements. However, measurements of the statistical quantities for the velocity have been found to closely resemble hot-wire measurements (mass flux) in subsonic jets [23] where the static temperature and ambient conditions were matched. In Fig. 3a, the streamwise (top) and radial (bottom) components of the fluctuating velocity field are presented, normalized by the jet exit velocity. The axial component is shown to peak between 8 and 10 jet diameters at around 15%, whereas the radial component peaks around 8%. Shear stress profiles of $u_1u_2/U_{\mathrm{cl}}^2$ are also shown in Fig. 3b with a peak around 0.7% of the jet exit velocity squared. These stress profiles agree well with the PIV measurements of Arakeri et al. [1] and Bridges [27], and in general show the same discrepancies with the LDV measurements of Lau et al. [20], which are attributed to the filtering effects inherent in PIV measurements as described by Westerweel [44]. Centerline statistical features of the axial velocity are shown in Fig. 3c whereby the potential core is shown to decay between five and six jet diameters. Arakeri et al. [1] showed that the mean axial velocity of a Mach 0.9 jet ($D = 2.2$ cm) decayed to 70% of the jet exit speed around $x/D = 12$, whereas the peak in the axial rms occurred around 10 jet diameters. Likewise, the centerline velocity of a Mach 0.6 jet ($D = 8.2$ cm) was shown to decay toward 60% by Narayanan et al. [45] with the axial rms velocity peaking similarly around 10 jet diameters. The current measurements are complementary to these investigations whereby the mean axial centerline velocity decays to roughly 65% of the jet's exit velocity at $x/D = 12$ with a maximum in the turbulence intensity at $x/D = 10$.

Figure 4 displays the components of the Reynolds stress tensor from the data acquired at the LAC in the ($r$–$\theta$) plane, normalized by the jet exit velocity squared. The profiles are plotted using shear layer coordinates $[\eta(x) = (r - r_{0.5})/x]$** and manifest linear growth

**The radial location $r_{0.5}$ is where the mean axial velocity is 50% of the jet exit velocity.

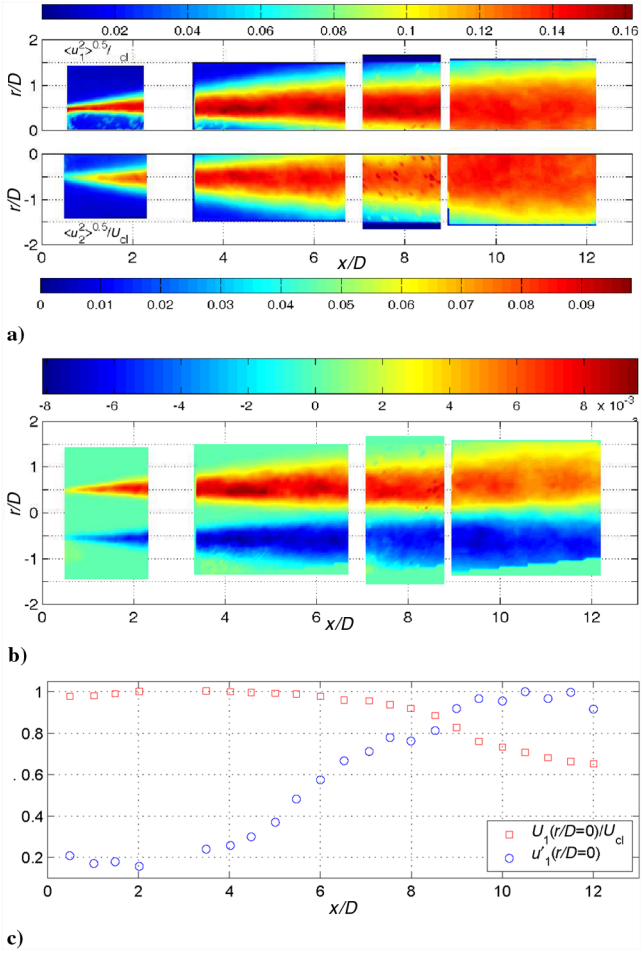


**Fig. 3 Stress profiles: a) velocity profiles of the axial (top) and radial (bottom) stresses; b) shear stress $\langle u_1 u_2 \rangle / U_{cl}^2$; and c) streamwise variation of the axial velocity's mean and turbulence intensity on the centerline where $u'_1$ has been normalized by its maximum value and is thus nondimensional.**

patterns for the high- and low-speed sides of the shear layer whereby the potential core is found to collapse between five and six jet diameters, similar to the measurements shown in Fig. 3c of the NCPA jet. The axial stress profile shown in Fig. 4a demonstrates a peak around 1.8%, in concert with other reported findings [20], whereas the radial stresses are under at 0.8%. The azimuthal component in Fig. 4c is slightly larger (0.9%) than the radial component, although they are quite close in this data set, both of which (radial and azimuthal) are nearly half the value of the axial component, which overall, reflects the highly anisotropic nature of the turbulent jet. In concert with the shear stress term presented in Fig. 3b from the NCPA jet, the shear stress term (axial–radial) in Fig. 4d exhibits a peak around 0.7% of the jet exit velocity squared. The peak energy manifest on the high-speed side of the shear layer is in good agreement with the measurements of others [18,46]. All normal and shear stresses at $x/D = 5$ are shown in Fig. 4f, demonstrating that $u_1 u_2$ is the only significantly nonzero component of the shear stresses. The spatial correlations generated from the $u_1 u_3$ shear stress term will be subsequently presented as it should not necessarily be discarded.

Where the peak energy is concerned, the spreading of the turbulent shear layer is visible in the normal components of the Reynolds stresses where the levels at $\eta(x) = 0$ are shown to increase until the collapse of the potential core, as was demonstrated by Narayanan et al. [45]. Interestingly, the shear stress component $u_1 u_2$ in Fig. 4d does not increase significantly, and maintains its profile well into the transition region of the flow. In hindsight, the overall agreement of these two data sets to those presented in the literature demonstrates the quality of the measurement techniques and of the facilities employed to construct a natural turbulent jet.

## V. Evolution of Two-Point Statistics

In this section, we will present two-point turbulent statistics throughout the measurement region and discuss the trends observed in the data. This will be done before evaluating the terms specific to the Lighthill source tensor and is necessary to demonstrate the characteristics of the high Reynolds number transonic jet. Where the azimuthal extent of these two-point correlations are concerned, the azimuthal symmetry of the jet is considered, and the correlations are only mapped over nonrepeating regions in space, that is between zero and $\pm\pi$. The mathematical form for calculating the normalized correlations of the axial–radial and radial–azimuthal data is as follows:

$$R_{ij}(x, r) = \frac{\langle u_i(x, r, t) u_j(x', r', t) \rangle}{\langle u_i(x, r, t)^2 \rangle^{0.5} \langle u_j(x', r', t)^2 \rangle^{0.5}}$$
$$R_{ij}(r, \theta) = \frac{\langle u_i(r, \theta, t) u_j(r', \theta', t) \rangle}{\langle u_i(r, \theta, t)^2 \rangle^{0.5} \langle u_j(r', \theta', t)^2 \rangle^{0.5}} \quad (9)$$

### A. Streamwise Velocity

Starting with the measurements from the NCPA, the two-point spatial correlations are evaluated across the jet's streamwise and radial plane. The origins of these correlations are fixed at three points in the radial direction ($r/D = 0.0$, 0.5, and 0.74) and two axial positions ($x/D = 4.0$ and $x/D = 8.0$), as shown in Figs. 5a and 5b, respectively.[††] At $r/D = 0.5$, the axial extent of the streamwise correlation increases from nearly 0.5 jet diameters at $x/D = 4$, to approximately one full jet diameter at $x/D = 8$. With the exception of regions within the potential core of the jet ($r/D = 0.0$), the streamwise domain over which the correlated region extends is about 2.5 times that of the radial domain. Where the radial extension of these correlations are concerned, they are shown to grow with the expanding shear layer but do not extend over the entire shear layer, in view of the radial correlations shown next. One interesting feature in this figure is the inclined nature of the correlation function in the shear layer regions of the flow, relative to the axis of the jet. This is also seen in the measurements of Arakeri et al. [1] and can be attributed to the straining of the large-scale turbulence structure.

The azimuthal dependence of these correlations are demonstrated in Fig. 6, consistent with the transonic jet measurements (hot wires) of Ukeiley and Seiner [23] and the incompressible jet measurements of Jung et al. [47]. Comparing the top ($x/D = 4$) and bottom ($x/D = 8$) profiles, the azimuthal extent of the streamwise spatial correlations in the outer part of the mixing layer at $x/D = 8$ are much larger when compared with the measurements observed at $x/D = 4$. The opposite is true in the potential core region where the correlated region has a larger azimuthal distribution at the upstream position. This is a well-known artifact of jet flows whereby the potential core region gives way to the expanding turbulent shear layer up until the collapse of the potential core.

### B. Radial Velocity

For the radial component of the two-point correlations (Fig. 7), the streamwise extent of the large-scale structure does not exhibit the same inclined behavior as the streamwise correlations (Fig. 5) and grows at a fairly uniform rate in this region of the flow. A more interesting feature is the radial extent of the correlation in the potential core region of the flow at $r/R = 0.0$ in Fig. 7a and 7b. The axial extent of this correlation is shown to have a spatial phase shift (in sign) of approximately one jet diameter at both $x/D = 4$ and 8, and is evidence of a compact well-organized flapping mode structure (a helical Fourier mode 1). This is consistent at both axial positions

[††]The origin for evaluating the correlations over the axial and radial plane will be the same in subsequent figures using the NCPA jet data with contour levels ranging between −0.5 and 1.0 with increments of 0.1.

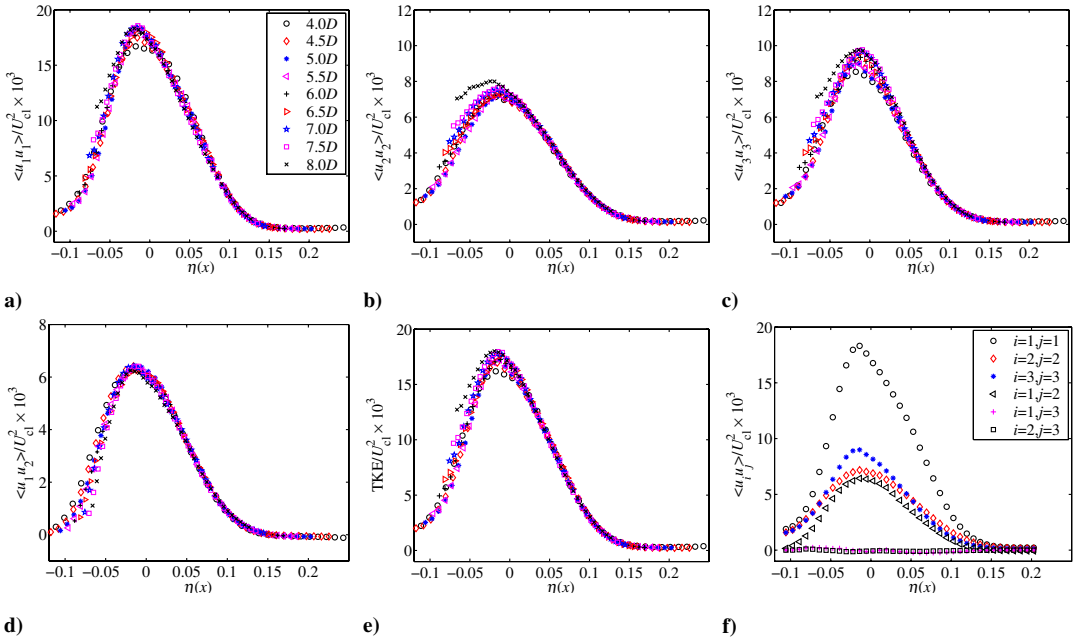


**Fig. 4 Radial distribution of individual Reynolds stress components: a) axial $i,j = 1$, b) radial $i,j = 2$; c) azimuthal $i,j = 3$; d) shear $i = 1, j = 2$; e) turbulent kinetic energy $0.5\langle u_1^2 + u_2^2 + u_3^2\rangle$; and f) survey of Reynolds stress components at $x/D = 5$.**

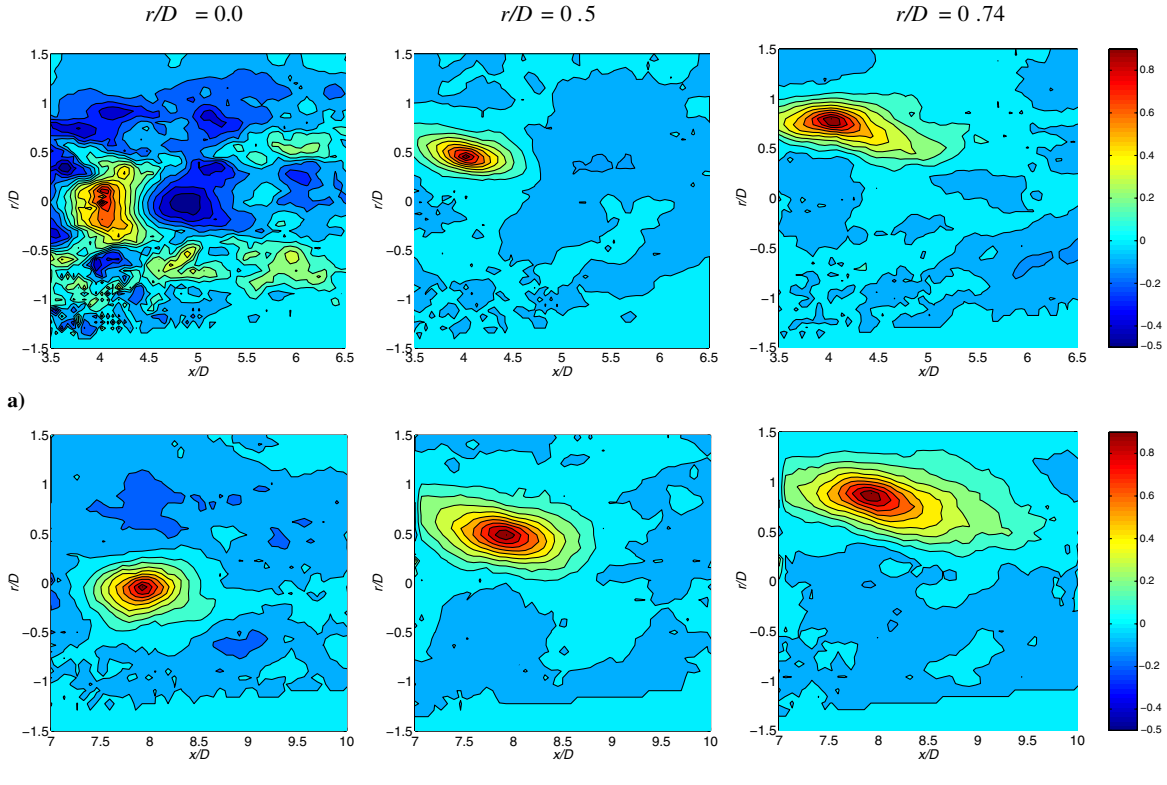


**Fig. 5 Normalized streamwise velocity correlation coefficients in the ($r$–$x$) plane at a) $x/D = 4.0$, and b) $x/D = 8.0$.**

shown. In the shear layer region ($r/D = 0.5$ and 0.74) at $x/D = 8.0$, the spatial extent of the correlation stretches to nearly one full jet diameter, from about half a jet diameter at $x/D = 4.0$. As one might expect, the radial component of the large-scale structures convecting through the shear layer accounts for more of the shear layer's growth than do the axial components.

Because the distribution of the radial correlations in the ($r$–$x$) plane (Fig. 7) demonstrate helical-type structures in the potential core regions of the flow, then the same should be expected of the radial correlations across the ($r$–$\theta$) plane. Considering first that in a cylindrical coordinate system, defined in a way that $+r$ and $-r$ (where $r/D$ is positive) represent fluid movements from the potential core to the shear layer and from the shear layer to the potential core,[‡‡] respectively, then for a helical-type structure, the radial component of the velocity vector should be opposite in sign for azimuthal

[‡‡]The opposite being true for the section of the jet where $r/D$ is negative.

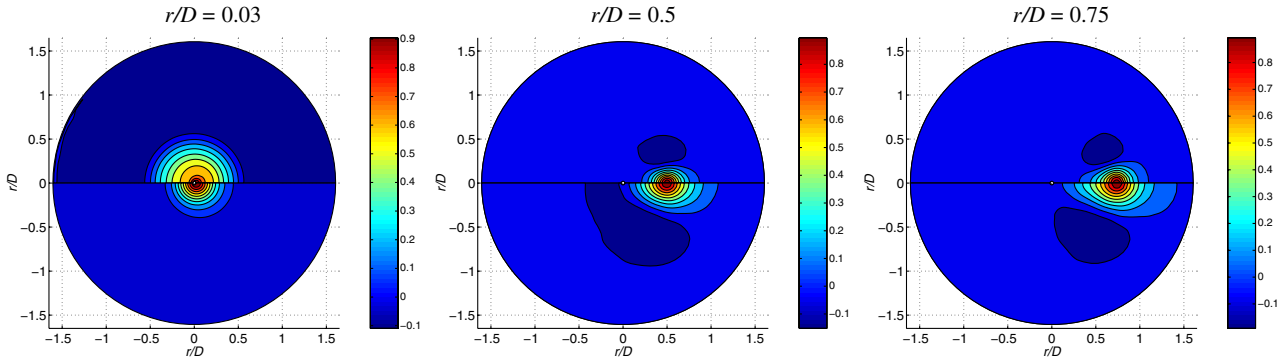


**Fig. 6 Normalized streamwise velocity correlation coefficients in the ($r$–$\theta$) plane at $x/D = 4$ (top) and $x/D = 8$ (bottom).**

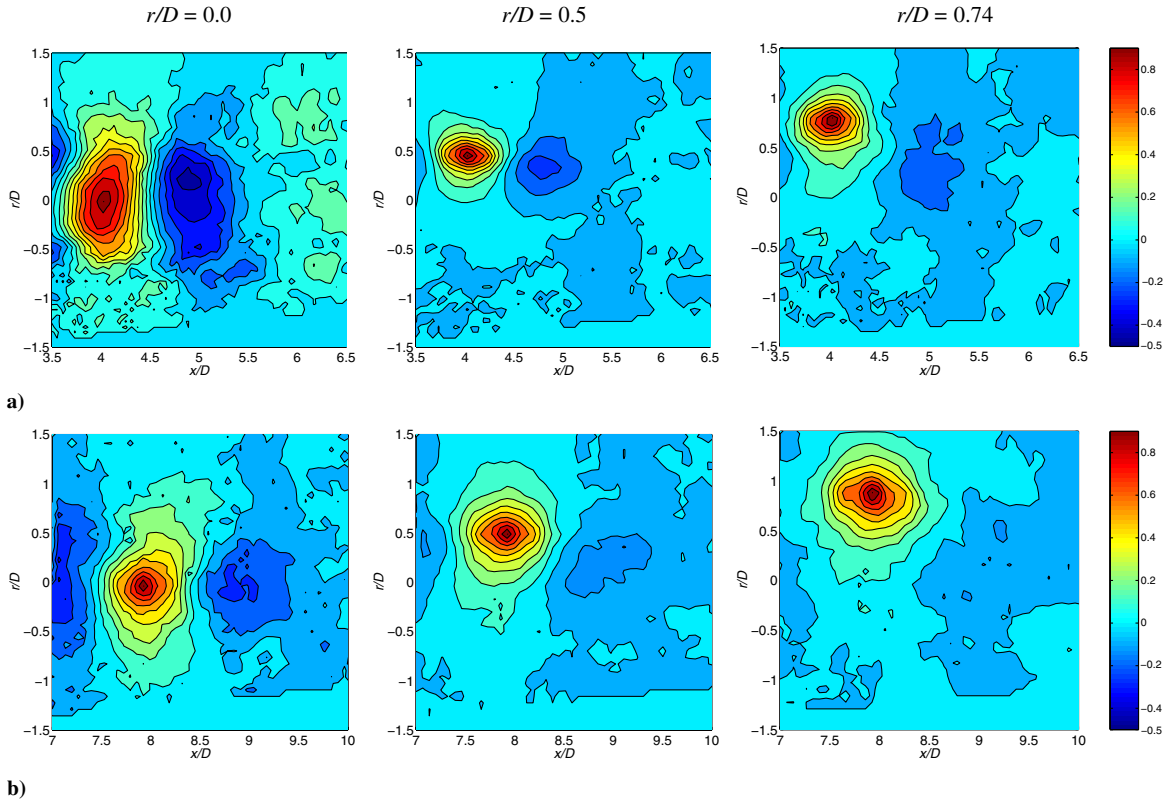


**Fig. 7 Normalized radial velocity correlation coefficients in the ($r$–$x$) plane at a) $x/D = 4.0$, and b) $x/D = 8.0$.**

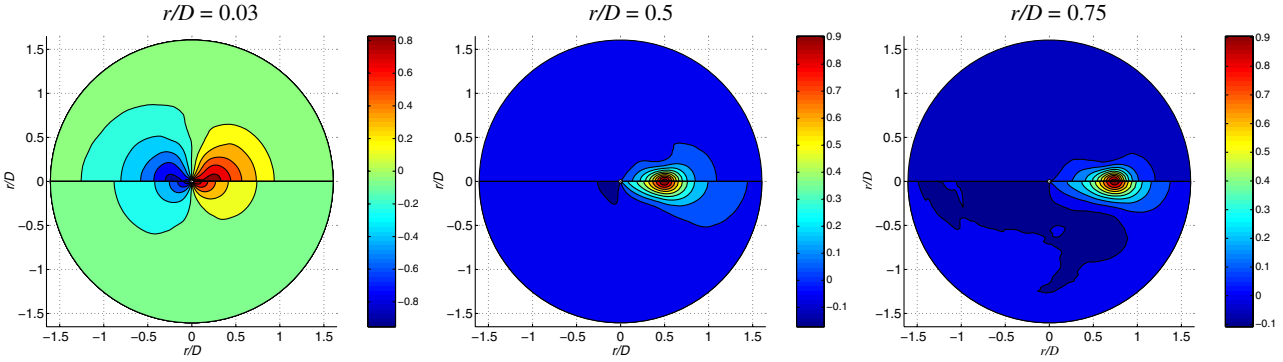


**Fig. 8 Normalized radial velocity correlation coefficients in the ($r$–$\theta$) plane at $x/D = 4$ (top) and $x/D = 8$ (bottom).**

separations 180 deg away from the point of origin. This is indeed the case as is shown in Fig. 8 at $r/D = 0.03$ where the radial extent of the radial correlation is opposite in sign with respect to the diametric disposition of the point of origin. The Fourier–azimuthal decomposition of the Mach 0.85 jet has been performed by Tinney et al. [33] using the correlations presented here and demonstrated a significant contribution to the turbulent energy from the helical mode structure at these Reynolds numbers and jet exit speeds when compared with the lower speed, lower Reynolds number flows presented by Jung et al. [47].

At $r/D = 0.5$ and 0.75 in Fig. 8 (where the points of origin are within the shear layer regions), the spatial extent of the correlations are shown to grow more in the radial direction than in the azimuthal direction where the differences in the downstream position are concerned. This small growth (azimuthally) results in the presence of higher Fourier–azimuthal modes that are commonly found in the low-speed (low-frequency) side of the turbulent jet's shear layer [23].

### C. Azimuthal Velocity

In light of the aforementioned normal stresses, the $(r–x)$ spatial distribution of the azimuthal correlation (Fig. 9) demonstrates a vector component of the large-scale turbulent structure which is more compact and less dispersive in space. Similar to the axial correlations shown in Fig. 5, the azimuthal correlations are inclined at an angle which appears to be around 20–30 deg from the jet axis (dashed line), however, it is much more pronounced here. This is an interesting artifact considering that the peak radiation of the pressure field that propagates into the far field has been shown to typically occur at an angle of 20–30 deg from the positive jet axis. Furthermore, the obliqueness of the correlation appears to have little dependence on the axial or radial position in the flow in view of the measurements in Figs. 9a and 9b. One interpretation of this behavior exhibited by these correlations is due to a helical structure associated with the azimuthal velocity. For origins on the centerline of the jet, there is a large correlated region which extends equally in the radial and streamwise directions while exhibiting features of an oblique structure in the shear layer. This behavior appears to be consistent throughout the entire streamwise domain studied.

The azimuthal extent of the azimuthal correlations are shown in Fig. 10 and are similar to the radial velocity correlations at $r/D = 0.0$, whereby the sign switching articulates the presence of a helical azimuthal mode structure in the potential core regions. The radial extent of these correlations are nearly half of those observed for the radial velocity. In the mixing layer, the spatial extension of the correlation azimuthally is similar to the $(r–x)$ distribution of the radial correlations illustrated in Fig. 7, thus demonstrating how the energy shifts to lower Fourier–azimuthal mode numbers after the end of the potential core [24].

### D. Shear Components

Although we have only considered so far the two-point correlations of the normal stresses, the shear stress components of the velocity field are presented here for completeness. In Fig. 11, the

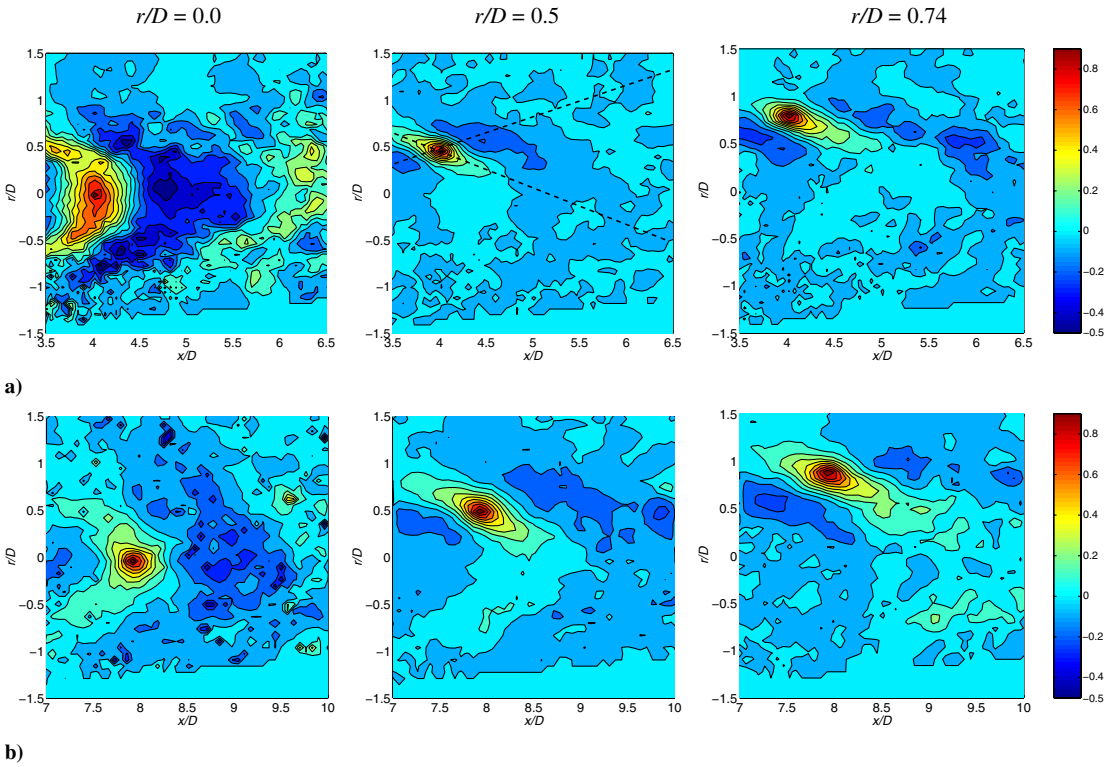


**Fig. 9 Normalized azimuthal velocity correlation coefficients in the $(r–x)$ plane at a) $x/D = 4.0$, and b) $x/D = 8.0$.**

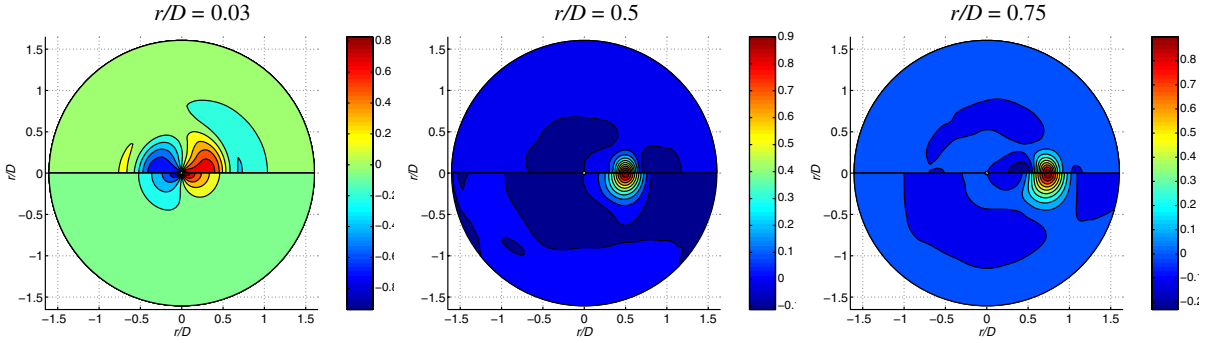


**Fig. 10 Normalized azimuthal velocity correlation coefficients in the $(r–\theta)$ plane at $x/D = 4$ (top) and $x/D = 8$ (bottom).**

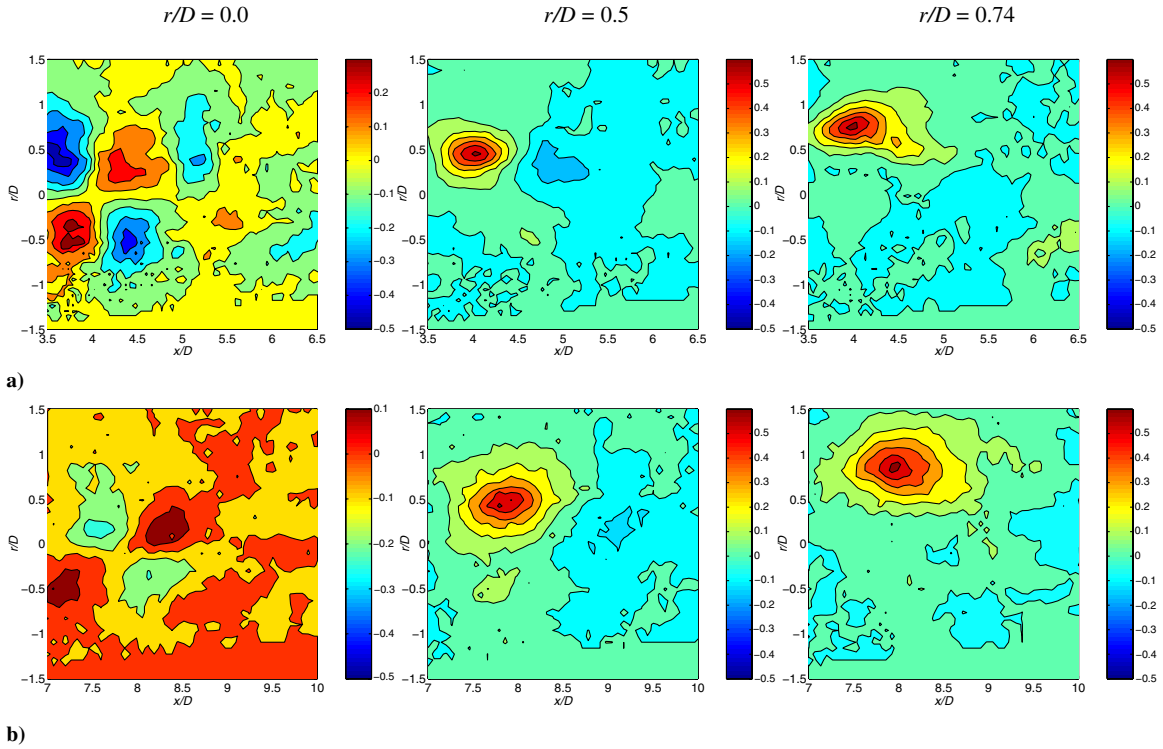


**Fig. 11 Normalized shear velocity correlation coefficients in the ($r$–$x$) plane at a) $x/D = 4.0$, and b) $x/D = 8.0$.**

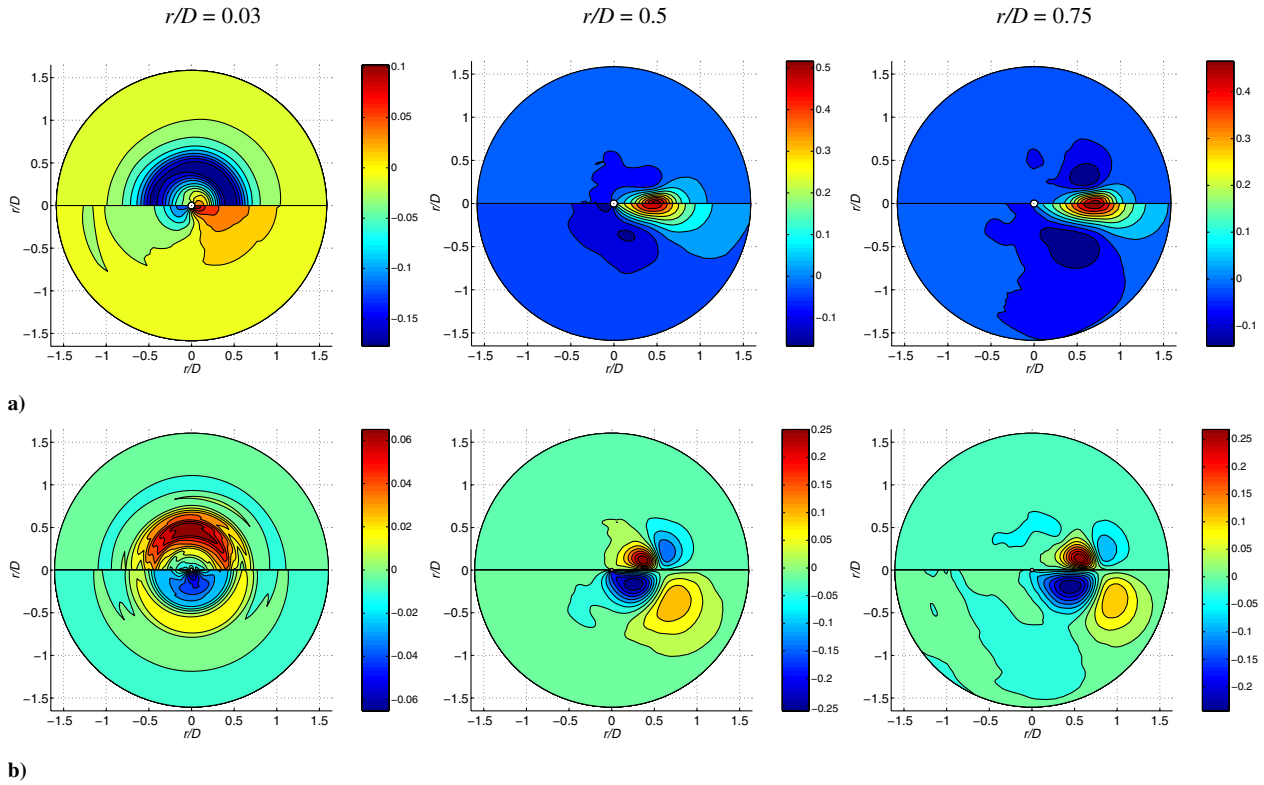


**Fig. 12 Normalized shear velocity correlation coefficients in the ($r$–$\theta$) plane at $x/D = 4$ (top) and $x/D = 8$ (bottom) for a) ($u_1u_2$), and b) ($u_1u_3$).**

$u_1u_2$ components illustrate similar characteristics to the radial correlations (Fig. 7) in the shear layer regions of the flow. The correlations at the jet's center ($r/D = 0.0$) show evidence of fluid being entrained before the point of origin, followed by an ejection of fluid from the potential core after the point of origin. The spatial separation between these events are on the order of one jet diameter at both axial stations, and is consistent with streamwise and radial correlations shown in Figs. 5 and 7. It should be noted that the sign of these correlations is an artifact of the coordinate system and that the relationship of the axial–radial shear stresses agree with the general theorem that $uv = -\nu_T(\partial U/\partial r)$.

The same phenomena is shown in Fig. 12a at $r/D = 0.03$, whereby the potential core region of the flow manifests a strong azimuthal correlation resulting from the passage of turbulent structures whose radial and axial components are phase aligned. This has been demonstrated by Citriniti & George [48] who reconstructed time-resolved slices through the ($r$–$\theta$) plane of the low-Reynolds number, low-speed jet and the eruption of highly correlated

structures through the flow's potential core regions followed by higher Fourier mode events in the low-speed side of the shear layer [49].

Figure 12b displays the streamwise–azimuthal velocity correlations in the ($r$–$\theta$) plane. One can see that the correlation between these two components is weak in the potential core region, but should not be so easily discarded in the shear layer regions as they appear to possess a fair percentage of the total turbulent velocity's energy. The fact that both of these correlations exhibited antisymmetric patterns implies that when the spatial volumes are integrated in Lighthill's analysis, these components will not contribute (or very little) when there is no time separation. This demonstrates the necessity for evaluating the space-time characteristics of these correlations to determine whether these events contribute significantly to the radiated noise field.

## VI. Quadrupole Correlations

To calculate the relative contributions of the different quadrupole self- and cross-correlations to the sound emitted in a given direction, Ribner [42] reformulated the Lighthill theory by postulating isotropic turbulence superposed on a mean flow. This is important, as the effects of convection and refraction, which are known to dominate the heart-shaped pattern of jet noise, can be corrected out to yield the small basic directivity of the eddy noise generators [42].

The process entails reducing the 36 possible quadrupole correlations to a distinct set of nine, nonvanishing correlation integrals, shown in Eq. (8) as $\langle \tilde{u}_i \tilde{u}_j \tilde{u}'_k \tilde{u}'_l \rangle$, that contribute to the axisymmetric noise pattern of a round jet. Decomposing the instantaneous field into mean and turbulence quantities ($\tilde{u}_i = U_i + u_i$), leads to the terms commonly known as "shear" and "self" noise components. The shear-noise (fast) components comprise interactions of the mean flow with the turbulence, $U_i U'_j \langle u_k u'_l \rangle$, whereas the self-noise (slow) components involve interactions of the turbulence with the turbulence $\langle u_i u_j u'_k u'_l \rangle$. Note that the primes in Ribner's formulation [42] comprise velocity terms that are functions of both spatial and temporal separations. With the current data set, only spatial separations can be examined. In the absence of temporal information, this may be misleading because the latter of the two demonstrates the frequency dependence of the space-time structure. However, one can still gain insight into the relative weights of the components by examining these correlations with spatial separations only, and in addition, this information can serve to help guide future analysis.

In the subsequent discussion, the nine different source terms will be analyzed to provide a basic understanding of their relative contribution to the overall noise generated by round jets. Whereas the spatial correlations have been shown to comprise inhomogeneous and anisotropic behavior, the evaluation of Ribner's terms are still exact. It is worth mentioning that the effects of the isotropic assumption are being evaluated by many such as Khavrahan [17], Seiner et al. [43], and Jordan and Gervais [18]. The measurements in the latter two studies mentioned have shown that using the isotropic assumptions overestimate the shear-noise terms and that the self-noise terms dominate shear-noise terms by up to a factor of 2.5 when the anisotropic shape of the jet structure is retained. Thus, by directly calculating these terms from the PIV measurement, one is able to neglect any assumptions that may be otherwise limiting and demonstrate their true spatial topology.

### A. Shear-Noise Terms

In the axisymmetric jet, the mean streamwise velocity is at least one order of magnitude greater than the radial or azimuthal velocities (Fig. 2). Therefore, the only significant shear-noise terms would be

$$U_1 U'_1 \langle u_1 u'_1 \rangle \qquad U_1 U'_1 \langle u_2 u'_2 \rangle \qquad U_1 U'_1 \langle u_3 u'_3 \rangle \tag{10}$$

Clearly, these terms will have similar behavior to what was discussed in the previous section where the two-point statistics are concerned and are illustrated in Fig. 13 using the $r$–$x$ plane data at $x/D = 4$. These shear-noise terms are normalized by $U_{cl}^4$ and the radial position of the origin is identified at the top of each column.

One can see from Fig. 13 that the azimuthal component ($U_1 U'_1 \langle u_3 u'_3 \rangle$) comprises the strongest correlation in all regions of the flow, except in the low-speed side of the shear layer ($r/D = 0.75$) where the azimuthal and streamwise correlations are maximally similar. It is interesting to point out that where the radial dependence of the origin is concerned, the correlations shown in Fig. 13 were determined to comprise the greatest levels using the origins at $r/D = 0.33$. Thus, the maximum shear-noise correlations (determined for all three components) are favorable toward the high-speed side of the shear layer. The significance of this, where the pressure field is concerned, has been investigated recently by Hall et al. [50] whereby the near-field pressure region surrounding a high-speed subsonic jet flow has been found to have a strong linear dependence, $\langle pu \rangle$, with the velocity field along the interfacial region of the flow between the potential core and the high-speed side of the shear layer. The same pressure velocity correlations were extended to quadratic relationships by Tinney et al. [40] to quantify the nonlinear dependencies, $\langle puu \rangle$. The results exhibited identical spatial dependencies between the linear and nonlinear correlations, although the linear term was shown to contain higher levels than the nonlinear term. Therefore, the findings reported here demonstrate important information concerning the near-field pressure and perhaps insight into the noise generating events of the flow. The shear-noise terms, with origins located further downstream (not shown), were quite similar to those shown here at $x/D = 4$; the major differences being slightly higher values over a slightly larger area.

### B. Self-Noise Terms

The last surviving self-noise terms (nine) that contribute to the noise pattern of the jet are written as follows:

$$\begin{gathered} \left\langle u_1^2 u_1'^2 \right\rangle \quad \left\langle u_1^2 u_2'^2 \right\rangle \quad \left\langle u_1 u_2 u'_1 u'_2 \right\rangle \quad \left\langle u_2^2 u_2'^2 \right\rangle \quad \left\langle u_1^2 u_3'^2 \right\rangle \\ \left\langle u_1 u_3 u'_1 u'_3 \right\rangle \quad \left\langle u_3^2 u_3'^2 \right\rangle \quad \left\langle u_2^2 u_3'^2 \right\rangle \quad \left\langle u_2 u_3 u'_2 u'_3 \right\rangle \end{gathered} \tag{11}$$

The spatial distribution of a subset of these correlations are shown in Fig. 14 at $x/D = 4$ and, in general, have smaller peak values than the shear-noise terms. Like the shear-noise terms, the origin in the radial direction was selected based on the maximum correlation value which was found to follow the lip-line of the jet at $r/D \sim 0.5$. This is different from the shear-noise terms (Fig. 13) whereby the maximum correlation was found to occur on the high-speed side of the mixing layer. For the self-noise terms, the normal stress correlations $\langle u_1^2 u_3'^2 \rangle$ and $\langle u_2^2 u_3'^2 \rangle$ were similar to the $\langle u_1^2 u_2'^2 \rangle$ correlation in Fig. 14, and so are not shown. Also, the spatial distribution of the shear stress correlation $\langle u_2 u_3 u'_2 u'_3 \rangle$ (not shown) was similar to the shear stress correlation $\langle u_1 u_3 u'_1 u'_3 \rangle$, although the latter of the two (shown in Fig. 14) contained a peak value of nearly twice that of the former. One can see from these correlations that, except for the shear stress term $\langle u_1 u_3 u'_1 u'_3 \rangle$ (and hence $\langle u_2 u_3 u'_2 u'_3 \rangle$), the correlations extend to the opposite side of the mixing layer. By comparing the relative amplitudes of these functions, it is clear that the dominant self-noise terms for the zero time delay case are the axial $\langle u_1^2 u_1'^2 \rangle$ and azimuthal $\langle u_3^2 u_3'^2 \rangle$ normal stresses.

## VII. Summary

The turbulent statistics as they relate to the Lighthill source terms were investigated in a high Reynolds number, Mach 0.85 axisymmetric jet flow. Specifically, the two-point spatial statistics were studied to determine trends in all three flow coordinates. The analysis comprised measurements from two separate experiments using stereo three-component PIV techniques, that is, one with the light sheet orientated in the streamwise direction ($r$–$x$) and one with the light sheet orientated perpendicular to the jet flow ($r$–$\theta$). The single-point statistics were in good agreement with previously measured flow quantities and demonstrated typical inhomogeneous

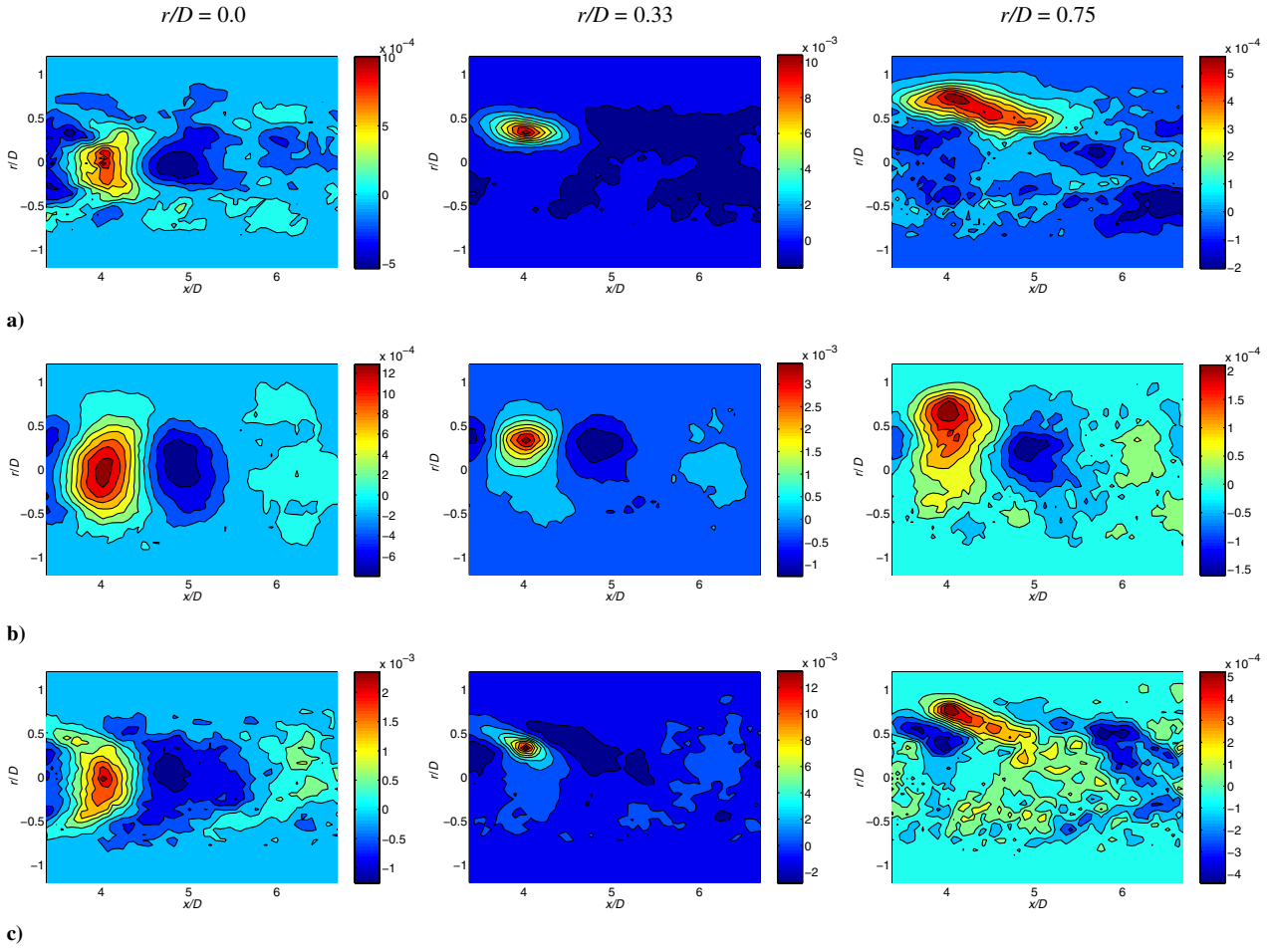


**Fig. 13 Shear-noise spatial correlations for a) streamwise $U_1U_1'\langle u_1u_1'\rangle$, b) radial $U_1U_1'\langle u_2u_2'\rangle$, and c) azimuthal $U_1U_1'\langle u_3u_3'\rangle$ components of velocity.**

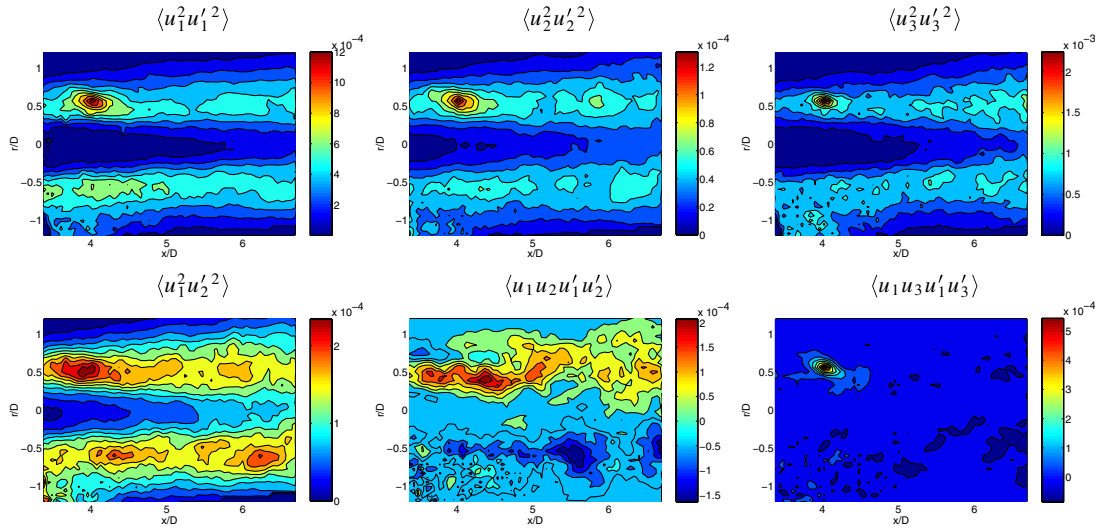


**Fig. 14 Self-noise spatial correlations normalized by $U_{cl}^4$ in the ($r$–$x$) plane, with the origin located at $x/D = 4$ and $r/D = 0.5$.**

and anisotropic behaviors of high-speed, high Reynolds number, subsonic jet flows.

Two-point statistics were also presented and illustrated the large spatial coherence in the potential core regions of the flow where the low-order structures of the flow are known to persist, whereas the azimuthal spatial correlations in the mixing layer regions demonstrated the characteristics that are typical of higher mode number (Fourier–azimuthal) events. A full vector decomposition of the velocity field was performed by Tinney et al. [33] and demonstrated that this is indeed the case, as has been shown by other investigators [24,47]. Where the axial and radial spatial dependence of the normal stresses are concerned, the axial and azimuthal components of velocity demonstrated an oblique-shaped structure in the mixing layer regions of the flow, whereas the radial normal stresses evolved downstream more uniformly.

Quadrupole correlations were also presented to demonstrate their spatial evolution in the radial and streamwise directions. From this, the peak energy for the shear-noise component at $x/D = 4$ was found

to reside on the high-speed side of the shear layer around $r/D = 0.33$, whereas the self-noise terms peaked along the lip-line at $r/D = 0.5$. Coincidentally, the axial $\langle u_1^2 u_1'^2 \rangle$ and azimuthal $\langle u_3^2 u_3'^2 \rangle$ normal stresses, and the combined normal stress term $\langle u_1^2 u_3'^2 \rangle$ comprised significantly greater correlation levels than all of the other nine self-noise terms.

Although this analysis has shed some insight into the noise sources in transonic jets following Ribner [42], space and time information is necessary to establish the link to the far-field noise. In this vane, conditional estimation techniques have been developed in conjunction with low-dimensional techniques [33,40] to permit time-resolved reconstructions of the jet's three-dimensional, large-scale structure. From this, the time dependence of the various quadrupole source terms can be calculated and the mechanisms responsible for jet noise can be assessed more thoroughly.

## Acknowledgments

This work has been partially funded by a grant from Air Force Office of Scientific Research, J. Schmisseur, technical monitor. The authors would also like to thank B. Jansen, R. Danforth, N. Murray, and L. Gui for assistance in acquiring and processing the particle imaging velocimetry measurements at the Jamie L. Whitten National Center for Physical Acoustics facility.

## References

[1] Arakeri, L., Krothapalli, A., Siddavaram, V., Alkislar, M. B., and Lourenco, L. M., "On the use of Microjets to Suppress Turbulence in a Mach 0.9 Axisymmetric Jet," *Journal of Fluid Mechanics*, Vol. 490, Aug. 2003, pp. 75–98.

[2] Freund, J. B., "Noise Sources in a Low-Reynolds Number Turbulent Jet at Mach 0.9," *Journal of Fluid Mechanics*, Vol. 438, July 2001, pp. 277–305.

[3] Lighthill, M. J., "On Sound Generated Aerodynamically 1: General Theory," *Proceedings of the Royal Society of London, Series A: Mathematical and Physical Sciences*, Vol. 211, March 1952, pp. 564–587.

[4] Lighthill, M. J., "On Sound Generated Aerodynamically 2: Turbulence as a Source of Sound," *Proceedings of the Royal Society of London, Series A: Mathematical and Physical Sciences*, Vol. 222, Feb. 1954, pp. 1–32.

[5] Crighton, D. G., "Basic Principals of Aerodynamic Noise Generation," *Progress in Aerospace Sciences*, Vol. 16, No. 1, 1975, pp. 31–96.

[6] Ffowcs–Williams, J. E., "Aeroacoustics," *Annual Review of Fluid Mechanics*, Vol. 9, 1977, pp. 447–468.

[7] Goldstein, M. E., *Aeroacoustics*, McGraw–Hill, New York, 1976.

[8] Ribner, H. S., "Perspectives on Jet Noise," *AIAA Journal*, Vol. 19, No. 12, 1981, pp. 1513–1526.

[9] Lilley, G. M., *Jet Noise: Classical Theory and Experiments*, edited by H. Hubbard, Vol. 1, NASA Reference Publ. 1258, 1991.

[10] Freund, J. B., "Noise-Source Turbulent Statistics and the Noise from a Mach 0.9 Jet," *Physics of Fluids*, Vol. 15, No. 6, 2003, pp. 1788–1799.

[11] Bogey, C., Bailly, C., and Juvé, D., "Noise Investigation of a High Subsonic, Moderate Reynolds Number Jet Using a Compressible Large Eddy Simulation," *Theoretical and Computational Fluid Dynamics*, Vol. 16, No. 4, 2003, pp. 273–297.

[12] Colonius, T., and Freund, J. B., "Application of Lighthill's Equation to a Mach 1.92 Turbulent Jet," *AIAA Journal*, Vol. 38, No. 2, 1999.

[13] Whitmire, J., and Sarkar, S., "Validation of Acoustic-Analogy Predictions for Sound Radiated by Turbulence," *Physics of Fluids*, Vol. 12, No. 2, 2000, pp. 381–391.

[14] Samanta, A., Freund, J. B., Wei, M., and Lele, S. K., "Robustness of Acoustic Analogies," *AIAA Journal*, Vol. 44, No. 11, 2006.

[15] Goldstein, M., "Generalized Acoustic Analogy," *Journal of Fluid Mechanics*, Vol. 488, Aug. 2003, pp. 315–333.

[16] Lilley, G. M., "On the Noise from Jets," AGARD CP-131, 1974.

[17] Khavaran, A., "Role of Anisotropy in Turbulent Mixing Noise," *AIAA Journal*, Vol. 37, No. 7, 1999, pp. 832–842.

[18] Jordan, P., and Gervais, Y., "Modelling Self- and Shear-Noise Mechanisms in Inhomogeneous, Anisotrpic Turbulence," *Journal of Sound and Vibration*, Vol. 279, Nos. 3–5, Jan. 2005, pp. 529–555.

[19] Harper-Bourne, M., "Jet Noise Turbulence Measurments," AIAA Paper 03-3214, 2003.

[20] Lau, J. C., Morris, P. J., and Fisher, M. J., "Measurements in Subsonic and Supersonic Free Jets Using a Laser Velocimeter," *Journal of Fluid Mechanics*, Vol. 93, No. 1, 1979, pp. 1–27.

[21] Morris, P. J., "Turbulence Measurements in Subsonic and Supersonic Axisymmetric Jets in a Parallel Stream," *AIAA Journal*, Vol. 14, No. 6, 1976, pp. 1468–1475.

[22] Stromberg, J. L., McLaughlin, D. K., and Troutt, T. R., "Flow Field and Acoustic Properties of a Mach Number 0.9 Jet at a Low Reynolds Number," *Journal of Sound and Vibration*, Vol. 72, No. 2, 1980, pp. 159–176.

[23] Ukeiley, L., and Seiner, J., "Examination of Large Scale Structures in a Transonic Jet Mixing Layer," ASME Paper FEDSM98-5234, 1998.

[24] Ukeiley, L., Seiner, J., and Ponton, M., "Azimuthal Structure of an Axisymmetric Jet Mixing Layer," ASME Paper FEDSM99-7252, 1999.

[25] Seiner, J., Ukeiley, L., and Ponton, M., "Jet Noise Source Measurements Using PIV," AIAA Paper 99-1869, 1999.

[26] Bridges, J., and Wernet, M., "Measurements of the Aeroacoustic Sound Source in Hot Jets," AIAA Paper 03-3130, 2003.

[27] Bridges, J., "Effect of Heat on Space-Time Correlations in Jets," AIAA Paper 06-2534, 2006.

[28] Siddon, T. E., "Noise Source Diagnostics Using Causality Correlations," AGARD CP-131, 1973.

[29] Seiner, J. M., and Reethof, G., "On the Distribution of Source Coherency in Subsonic Jets," AIAA Paper 74-0004, 1974.

[30] Schaffar, M., "Direct Measurements of Axial Correlations in Jet Velocity Fluctuations and Far Field Noise Near the Axis of Cold Jets," *Journal of Sound and Vibration*, Vol. 64, No. 1, 1979, pp. 73–83.

[31] Juvé, D., Sunyach, M., and Comte-Bellot, G., "Intermittency of Noise Emissions in Subsonic Cold Jets," *Journal of Sound and Vibration*, Vol. 71, No. 3, 1980, pp. 319–332.

[32] Thurow, B., Hileman, J., Lempert, W., and Samimy, M., "Technique for Real-Time Visualization of Flow Structure in High-Speed Flows," *Physics of Fluids*, Vol. 14, No. 10, Oct. 2002, pp. 3449–3552.

[33] Tinney, C. E., Ukeiley, L. S., and Glauser, M. N., "Evolution of the Most Energetic Modes in a High Sub-Sonic Mach Number Turbulent Jet," AIAA Paper 05-0417, Jan. 2005.

[34] Ponton, M. K., Seiner, J., Ukeiley, L., and Jansen, B., "New Anechoic Chamber Design for Testing High Temperature Jet Flows," AIAA Paper 01-2190, Jan. 2001.

[35] Gui, L., and Wereley, S., "Correlation Based Continuous Window-Shift Technique to Reduce the Peak-Locking Effect in Digital PIV Image Evaluation," *Experiments in Fluids*, Vol. 32, No. 4, April 2002, pp. 506–517.

[36] Wereley, S., and Gui, L., "Correlation Based Central Difference Image Correction (CDIC) Method and Application in a Four-Roll Mill Flow PIV Measurement," *Experiments in Fluids*, Vol. 34, No. 1, Jan. 2003, pp. 42–51.

[37] Mann, R., "Turbulence Properties of a Mach 0.85 Jet," Ph.D. Dissertation, Univ. of Mississippi, University, MS, 2006.

[38] Tinney, C. E., Hall, A., Glauser, M. N., Ukeiley, L. S., and Coughlin, T., "Designing an Anechoic Chamber for the Experimental Study of High Speed Heated Jets," AIAA Paper 04-0010, Jan. 2004.

[39] Tinney, C. E., Ukeiley, L. S., and Glauser, M. N., "Low-Dimensional Characteristics of Subsonic Jet Flows," *Journal of Fluid Mechanics*, pp. 1–28 (Currently in review).

[40] Tinney, C. E., Jordan, P., Hall, A. M., Delville, J., and Glauser, M. N., "Time-Resolved Estimate of the Turbulence and Source Mechanisms in a Subsonic Jet Flow," *Journal of Turbulence*, (to be published).

[41] Proudman, I., "Generation of Noise by Isotropic Turbulence," *Proceedings of the Royal Society of London, Series A: Mathematical and Physical Sciences*, Vol. 214, No. 1116, Aug. 1952, pp. 119–132.

[42] Ribner, H. S., "Quadrupole Correlations Governing the Pattern of Jet Noise," *Journal of Fluid Mechanics*, Vol. 38, No. 1, Aug. 1969, pp. 1–24.

[43] Seiner, J., Ukeiley, L., Ponton, M., and Jansen, B. J., "Progress in Experimental Measure of Turbulent Flow for Aeroacoustics," AIAA Paper 02-2402, 2002.

[44] Westerweel, J., "Effect of Sensor Geometry on the Performance of PIV Interrogation," *9th International Symposium on Laser Techniques Applied to Fluid Mechanics*, Springer, Lisbon, Portugal, 1998, pp. 37–55.

[45] Narayanan, S., Barber, T., and Polak, D., "High Subsonic Jet Experiments: Turbulence and Noise Generation Studies," *AIAA Journal* Vol. 40, 2003, pp. 430–437.

[46] Hussain, A. K. M. F., and Clark, A. R., "On the Coherent Structure of the Axisymmetric Mixing Layer: a Flow-Visualization Study," *Journal of Fluid Mechanics*, Vol. 104, 1981, pp. 263–294.

[47] Jung, D., Gamard, S., and George, W. K., "Downstream Evolution of the Most Energetic Modes in a Turbulent Axisymmetric Jet at High Reynolds Number, Part 1: the Near-Field Region," *Journal of Fluid*

*Mechanics*, Vol. 514, Sept. 2004, pp. 173–204.
[48] Citriniti, J., and George, W., "Reconstruction of the Global Velocity Field in the Axisymmetric Mixing Layer Using the Proper Orthogonal Decomposition," *Journal of Fluid Mechanics*, Vol. 418, Sept. 2000.
[49] Glauser, M., and George, W., "Orthogonal Decomposition of the Axisymmetric Jet Mixing Layer Including Azimuthal Dependence," *Advances in Turbulence*, edited by G. Comte-Bellot and J. Mathieu, Springer–Verlag, New York, 1987.
[50] Hall, A. M., Glauser M. N., and Tinney, C. E., "Experimental Investigation of the Pressure-Velocity Correlation of a $M = 0.6$ Axisymmetric Jet," AIAA Paper 05-5294, May 2005.

R. Lucht
*Associate Editor*